Journal of Fiber Bioengineering and Informatics 8:3 (2015) 593–601
doi:10.3993/jfbim00150

Film Flow Field Analysis of Hydrodynamic Polishing Based on FLUENT ⋆

Xiulian Zheng [a], Rui Zhang [b], Li Zhang [b,*], Mingsheng Jin [b]

[a] *Quzhou College, Quzhou 324000, China*

[b] *Key Laboratory of E and M, Zhejiang University of Technology, Ministry of Education and Zhejiang Province, Hangzhou 310014, China*

Abstract

The characteristics of film flow field have important effects on the quality of hydrodynamic polishing. Oriented preparation requirements of amorphous film substrate, in order to further study the floating height of hydrodynamic polishing base plate in working conditions, the mathematical model is established and the theoretical analysis has been carried out for the wedge hydrodynamic floating polishing base plate. The relationship between buoyancy and floating height is researched. The floating height is calculated under the known loads, and then the pressure distribution along the circumferential direction of base plate is analyzed. Film flow field is simulated and analyzed using the FLUENT based on the calculated floating height. It indicts that the bearing capacity of wedge combination plane decreases with the increase of floating height, and the downward trend slows down gradually. The pressure peak distributes near the interface of wedge flow field and parallel flow field. Through the pressure distribution comparison of simulation and calculation, the correctness of the mathematical model and simulation method is verified.

Keywords: Film Flow Field; Hydrodynamic Polishing Base Plate; Pressure Distribution; Buoyancy; FLUENT

1 Introduction

Amorphous alloy material is one of the most popular areas in the condensed matter physics over the past decade [1]. The vast majority of amorphous alloys have high strength and hardness. It is widely used in the field of construction materials and micro-devices. Vapor condensation method is a common method for preparing amorphous films, and the substrate is indispensable material during the preparation of amorphous film, what is more, the quality of substrate will seriously affect the surface morphology of the amorphous film. And that, in order to obtain a

⋆Project supported by the National Nature Science Foundation of China (No. 51575493, 51205358), Zhejiang Provincial Nature Science Foundation (No. Y15E050069), and Zhejiang Provincial Science Technology Department of China (No. 2014C31021).

*Corresponding author.
Email address: zhanglihz@163.com (Li Zhang).

1940–8676 / Copyright © 2015 Binary Information Press & Textile Bioengineering and Informatics Society
September 2015

thin, defect-free and good adhesion's alloy film, it asks for a substrate having ultra smooth surface without injury, avoiding mechanical damage, excessive corrosion and other factors which having impact on the surface [2], so, conventional chemical mechanical polishing technology is not fully suitable for the ultra-precision polishing of amorphous film substrate.

Hydrodynamic polishing can meet processing requirements of high flat surface and can achieve a high degree of reproducibility. Y. T. Su et al. conduct a deep research for hydrodynamic polishing [3–7]. Because of the high-speed rotary of the cutting tools, it generates hydrodynamic effects between the tool and the workpiece because of the wedge effect, which forms defibrination film between the tool and the workpiece. The abrasive in the film flow field will be effected by the shear stress of the flow field, and the shear stress will drive the abrasive to process the surface of the workpiece. By lubrication theory [8] and polishing mechanism known [9], through controlling the operating parameters of the film flow field between tool and workpiece and the characteristics between tools and workpiece, the processing characteristics of hydrodynamic polishing can be grasped fully.

This paper analyses the hydrodynamic floating polishing film flow field based on the two-dimensional simulation of FLUENT according to the hydrodynamic theory in order to further study the floating upward height of the hydrodynamic floating polishing base plate. The study object of this paper is wedge hydrodynamic floating polishing base plate. The simplified model is built based on its symmetry and the pressure of various positions in the flow field is calculated with Reynolds equation. Then the buoyancy of the flow field is got and verified that it can overcome gravity of the base plate. The floating upward height is got. Based on the calculating results, the flow field simulation of hydrodynamic floating polishing base plate is fulfilled by FLUENT. Through the pressure distribution comparison of simulation and calculation, the correctness of the mathematical model and simulation method is verified.

2 Hydrodynamic Floating Polishing Base Plate Model

The structure of the hydrodynamic floating polishing base plate is shown in Fig. 1. The main feature of the base plate is symmetrical to the center, and it is constituted by some same combined planes around the circumferential direction. The width in the radial direction of the combined planes is L, the length along the circumferential direction is B, what is more, the length of bevel is B_1, and the length of plane is B_2. In the case of that L is smaller than radius, the top view of combined planes can be seen as rectangle of which length is B and width is L. In the working condition, the hydrodynamic floating polishing base plate is fixed in the relative position of the horizontal plane, and the polishing plate below rotates. Because L is smaller than radius, the rotation of polishing plate can be seen as translation relatively to combined planes. Its speed is the line speed of that midpoint of L. It will produce a wedge fluid between combined plate and the working surface of polishing plate. The fluid which is driven by polishing plate flows in from the slope port of combined plane, then flows out from the other end of the plane. Based on the forming mechanism of hydro hydrodynamic [9], in a convergence space, incompressible fluid will form hydrodynamic when the fluid flows from a bigger inlet to a smaller outlet. Because the size of each combined plane is same and distributed uniformly along the circumference, so only need to analyze one of the combined planes' working situation, then the working situation of the entire base plate can be got. The simplified model is shown in Fig. 2.

In Fig. 2, W is the own weight of the base plate, h_1 is the thickness of the inlet's fluid, h_2 is

the height of the floating base plate, which is the thickness of the outlet's fluid, U is the speed of movement of the polishing plate, and a rectangular coordinate system has been established.

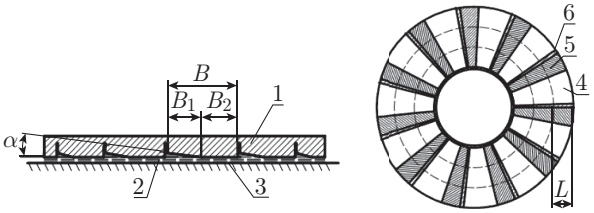

1—Hydrodynamic floating polishing base plate; 2—Polishing fluid; 3—Polishing plate
4—Slope in the base plate; 5—Plane in the base plate; 6—Groove

Fig. 1: Structural diagram of hydrodynamic floating polishing base plate

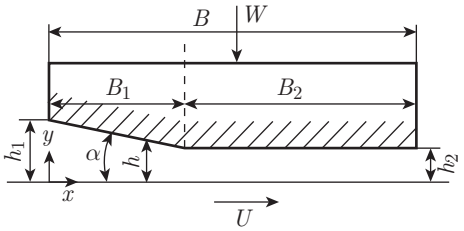

Fig. 2: Structural diagram of combined plane

3 Theoretical Analysis

3.1 Reynolds Equation

For the case of that the load is stable and the axial sliding bearing is lubricated by the incompressible Newtonian fluid, the most common form of Reynolds equation is shown in Eq. (1) [10]:

$$\frac{\partial}{\partial x}\left(\frac{h^3}{\mu}\frac{\partial p}{\partial x}\right)+\frac{\partial}{\partial z}\left(\frac{h^3}{\mu}\frac{\partial p}{\partial z}\right)=6U\frac{\partial h}{\partial x} \tag{1}$$

The working principle of hydrodynamic floating polishing base plate is similar with the axial sliding bearing, so the Reynolds equation above is also suitable for polishing base plate model.

If it is assumed that the combined plane is infinite in the direction of width, it also means that the pressure has no change in the z direction, so, Eq. (1) is changed below.

$$\frac{\partial}{\partial x}\left(\frac{h^3}{\mu}\frac{\partial p}{\partial x}\right)=6U\frac{\partial h}{\partial x} \tag{2}$$

3.2 Boundary Conditions

Pressure boundary conditions: both ends of the combined plane, that is the inlet and outlet of fluid are set to pressure boundary, and the pressure values are 0, the public pressure of the interface of wedge flow field and parallel flow field is P_0:

Inlet of fluid: $p|_{s1} = 0$

Outlet of fluid: $p|_{s2} = 0$

The interface of wedge flow field and parallel flow field:

$$p|_{s3} = p_0 = 6\mu U B_2 \frac{h_0 - h_2}{h_2^3}$$

Kinematical boundary condition: the workpiece of polishing plate is kinetic, so the lower surface of flow field is set to velocity boundary, the value of velocity is U.

3.3 Thickness of Fluid Film

As shown in Fig. 2, the flow field is consisted by wedge flow field and parallel flow field. In the parallel flow field, the thickness of fluid film is unchanged. In the wedge flow field, the thickness of fluid film varies with the change of x, that is:

For the area $B_1, h = \alpha x + h_2$;

For the area $B_2, h = h_2$;

For the area B_1, using the forms of $h_1 - h_2$ to represent α;

$h = \alpha x + h_2 = (h_1 - h_2)/B_1 x + h_2$

3.4 Static and Dynamic Analysis

Solving Eq. (2) discretely, the pressure distribution of the whole flow field is shown below:

For the area B_1,

$$p_1 = \int_{h_2}^{h_1} \frac{6\mu U B_1}{h_1 - h_2} \left(\frac{1}{h_2} - \frac{h_0}{h_3} \right) dh \tag{3}$$

For the area B_2,

$$p_2 = \int (B_1)^B 6\mu U (B - x) \frac{h_2 - h_0}{h_2^3} dx \tag{4}$$

In Eq. (3) and Eq. (4), $h_0 = \frac{2h_1h_2(B_1h_2+B_2h_2)}{(h_1+h_2)(B_1h_2+2B_2h_1^2/(h_1+h_2))}$ is the thickness of fluid film when the pressure is maximum.

The expression of P_0 is only a function of position h, so p is continuous in the boundary. The buoyancy of corresponding combined plane is:

$$W = \int_{h_2}^{h_1} L p_1 \frac{B_1}{h_1 - h_2} dh + \int_{B_1}^{B} L p_2 dx \tag{5}$$

In order to study the relationship between the buoyancy and the floating height of base plate intuitively, the MATLAB is used to program and calculate. The parameters of the hydrodynamic floating polishing base plate which are using for calculation is shown in Table 1.

The load of the base plate is its own weight. The weight of the entire base plate is 49 N, which is assigned to 12 combined planes averagely, so the load of each combined plane is 4.08 N.

Table 1: Essential parameters of hydrodynamic polishing base plate

Radius of base plate R/mm	100
Thickness of base plate H/mm	20
Weight of base plate G/mm	49
Width of combined plane L/mm	40
Length of combined plane B/mm	40
Length of slope B_1/mm	16
Length of plane B_2/mm	24
Inclination angle of slope α/rad	0.0624
Linear velocity of polishing plate $U/(\mathrm{m}\cdot\mathrm{s}^{-1})$	2
Viscosity of polishing solution $\mu/(\mathrm{Pa}\cdot\mathrm{s})$	0.00152
Density of polishing solution $\rho/(\mathrm{kg}\cdot\mathrm{m}^{-3})$	1001

The result of Eq. (5) which is computed by MATLAB is shown in Fig. 3.

In Fig. 3, the blue curve represents the relationship of buoyancy and floating height. This curve shows that combined plane's buoyancy reduces with the increase of the floating height h_2. The tendency of decline gradually slows, when $h_2 < 60$ μm, the buoyancy reduces sharply. When $h_2 > 60$ μm, the decline is not obvious.

In Fig. 3, the red dashed line represents the load of combined plane. The abscissa of the intersection of the two lines is shown as 46 μm, if $h_2 < 46$ μm, the buoyancy is bigger than load, the base plate will float upward, if $h_2 > 46$ μm, the buoyancy is smaller than load, the base plate will sink. Only when $h_2 = 46$ μm, the buoyancy of combined plane equal to weight of load. In conclusion, when the parameters of base plate is fixed, the floating height of base plate is 46 μm.

Based on the analysis above, in the case of that the floating height h_2 is 46 μm, analyzing the pressure distribution of combined plane along the direction x, the pressure distribution curve of Eq. (3) and (4) computed by MATLAB is shown as Fig. 4.

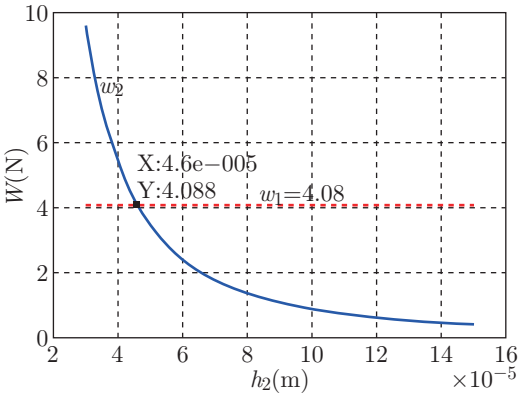

Fig. 3: Relationship of floating height and bearing capacity

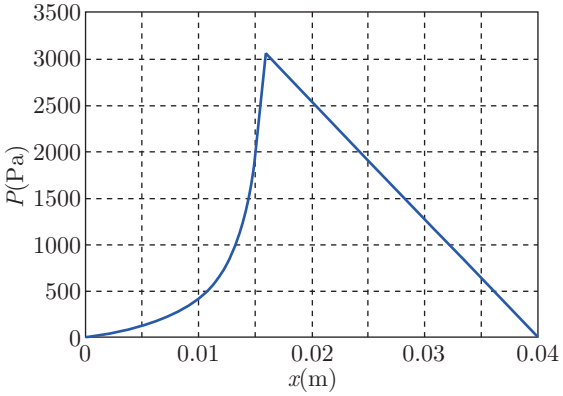

Fig. 4: Pressure distribution diagram of direction x

In Fig. 4, the pressure along the wedge flow field and rate of change is bigger and bigger. The pressure of interface of wedge and plane is maximum, the max value is 3050 Pa. The pressure decreases to 0 linearly when it passes the interface.

4 Establishing the Simulation Model of Film Flow Field

The parameters of hydrodynamic floating polishing base plate using for FLUENT simulation is shown in Table 1, in the other hand, $h_2 = 46$ μm. Establishing the model and meshing by GAMBIT, as Fig. 5 shows, the number of grids of flow field is 13591.



Fig. 5: The grid structure of flow field

Some assumptions about the model: (1) The fluid will be seen as incompressible fluid and a two-dimensional steady-state flow inside the wedge flow field. (2) There is no heat exchange between fluid and wall. The heat produced by high-speed motion is taken away through fluid. (3) The inertial force of the polishing solution is negligible, and the boundary pressure of fluid solution is zero. (4) No relative sliding between the fluid and solid. (5) The value of Re through computing is smaller than 2000, so the flow field is laminar flow, therefore, the flow field inside the combined planes is solved by laminar flow model. In the process of motion, thermal deformation of combined planes does not consider. So, viscous model set to Laminar.

Setting boundary conditions: Setting the boundary conditions of flow field's inlet as pressure inlet, setting the initial gauge pressure and gauge total pressure as 0; Setting the boundary conditions of flow field's outlet as pressure outlet, setting gauge total pressure as 0; Setting the upper surface as static wall, setting the lower surface as moving wall, and setting the absolute speed as 2 m/s.

5 Results and Analysis of Simulation

Because that the size of the model in Y direction is very small, the size in X direction is relatively much bigger, so the entire model belongs to slender model. In order to see the change of each parameter in the Y direction, the images which are simulated by FLUENT will also be processed by TECPLOT.

Fig. 6 is the velocity distribution of flow field, it is obvious that the velocity is maximum in the lower surface of the model, which is 2 m/s; The velocity is minimum in the upper surface of the model, which is always 0. The velocity distribution in the wedge flow field is relatively complex. It occurs low speed countercurrent in a certain area because of the slope.

Fig. 7 is the total pressure distribution of flow field. Fig. 7 (a) is the two-dimensional distribution contours of the total pressure in the flow field. It can be seen that the pressure gradually increases from zero at the inlet of flow field, but the increasement near the inlet is small, after 0.01 m, the increasement is obviously bigger, near 0.016 m, that is, the pressure reaches maximum near the interface of wedge flow field and parallel flow field, then in the parallel flow field, the pressure gradually decreases to zero. Fig. 7 (b) is the XYPlot curve of the total pressure of flow field, in the figure, the wallup represents upper surface of flow field, walldown represents lower surface of flow field. The key point of this paper is the upper surface of flow field. The change of pressure in the x direction can be seen directly. It appears that the maximum is 3200 Pa at 0.016 m, at the same time, it appears that the pressure decreases sharply near a small range of maximum, the value of decrease is nearly 150 Pa. The pressure decreases linearly in the parallel flow field.

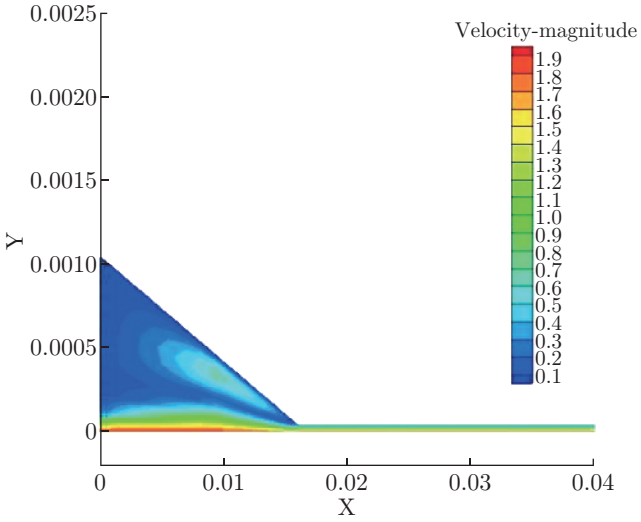

Fig. 6: Velocity distribution of flow field

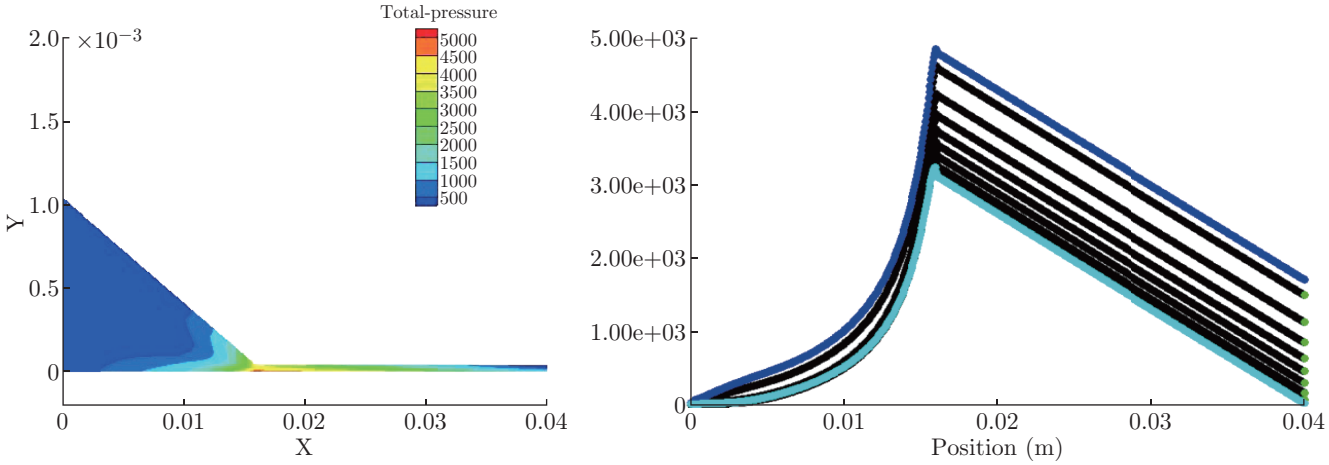

(a) Distribution contours of the total pressure

(b) XYPlot curve of the total p ressure

Fig. 7: Total pressure distribution of flow field

Importing the date of the pressure distribution of wallup in Fig. 7 (b) into MATLAB, then making the curve and comparing with the curve in Fig. 6, the result is shown in Fig. 8.

In Fig. 8, the red curve is the pressure curve which is simulated by FLUENT, and the blue curve is the pressure curve which is wrought out by theoretical calculation. The pressure distribution of the two curves are very similar, they are both parabolic rising from the inlet and reaching the maximum at 0.016 m, after this, the two curves decline linearly until the outlet. In the first half of the two curves, the change rate of simulated pressure distribution curve is a bit bigger than theoretical pressure distribution curve. The maximum of simulated pressure curve is bigger about 120 Pa than the maximum of theoretical pressure curve, however, the offset of the two curves do not exceed 150 Pa. In the second half of the two curves, the two curves are almost coincident, the maximum offset do not exceed 20 Pa. To sum up, the results of mathematic model and simulation model are same basically. The validity of mathematic model is verified.

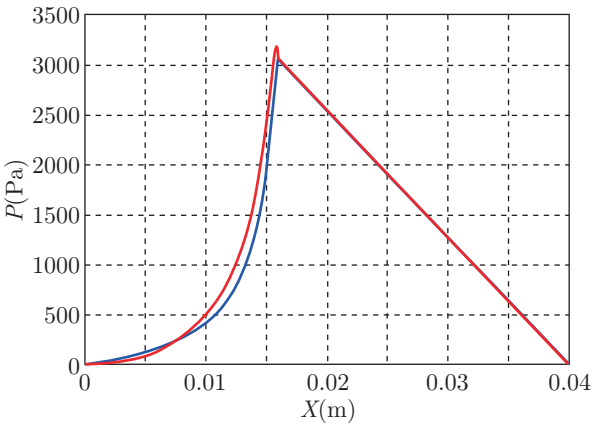

Fig. 8: Pressure distribution comparison of simulation and calculation

6 Conclusions

(1) The bearing capacity of the combined plane declines with the rise of floating height h_2, and the tendency of decline gradually slows. When $h_2 < 60$ μm, the bearing capacity declines sharply with the rise of h_2; When $h_2 > 60$ μm, the decline is already not obvious.

(2) In the case that the parameters of the base plate have already been given in this paper, the floating height of the base plate is 46 μm.

(3) The pressure increases gradually from 0 at the inlet of flow field, but the tendency of increase is much small near the inlet; After 0.01 m, the tendency of increase becomes bigger obviously; Near 0.016 m, that is near the interface of wedge flow field and parallel flow field, the pressure reaches maximum; Then, the pressure decreases to 0 in the parallel flow field.

(4) The upper surface of the film flow field is not affected by hydrodynamic pressure, so it can be considered that the upper surface of the film flow field is only affected by static pressure.

References

[1] P. L. Maitrepierre, Structure of amorphous Ni-Pd-P and Fe-Pd-P alloys [J], Journal of Applied Physics, 40(12), 1969, 4826-4834

[2] Xiaoming Ge, PdNiP Preparation and Growth Mechanism of Amorphous Alloy Films [M], Zhejiang University, 2007

[3] T. C. Hung, S. H. Chang, C. H. Ding et al., Improvement of residual error in hydrodynamic polishing by recursive error compensation strategy [J], Microelectronic Engineering, 93, 2012, 27-34

[4] T. C. Hung, C. H. Ding, Small-wavelength form error compensation during hydrodynamic polishing [J], International Journal of Machine Tools and Manufacture, 51(12), 2011, 880-888

[5] Y. T. Su, T. C. Hung, Y. Y. Chang, C. C. Horng, An experimental study on tool wears of hydrodynamic polishing process [J], Wear, 246(1-2), 2000, 117-129

[6] Y. T. Su, T. C. Hung, Y. Y. Chang, On machining rate of hydrodynamic polishing process under semi-contact lubricating condition [J], Wear, 220(1), 1988, 22-33

[7] Y. T. Su, C. C. Horng, S. Y. Wang et al., Ultra-precision machining by the hydrodynamic polishing process [J], International Journal of Machine Tools & Manufacture, 36(2), 1996, 275-291

[8] Y. T. Su, S. Y. Wang, J. S. Hsiau, On machining rate of hydrodynamic polishing process [J], Wear, 188(1-2), 1995, 77-87

[9] Shizhu Wen et al., Principles of Tribology [M], Tsinghua University Press, 1990

[10] O. Pinkus, B. Sternlicht, Theory of Hydrodynamic Lubrication [M], Machinery Industry Press, 1980